Contrib Mineral Petrol (1994) 118:169–181
© Springer-Verlag 1994

Rebecca A. Lange · Katharine V. Cashman
Alexandra Navrotsky

Direct measurements of latent heat during crystallization and melting of a ugandite and an olivine basalt

Received: 19 October 1993 / Accepted: 3 May 1994

Abstract Step-scanning calorimetric measurements using a Setaram HT1500 calorimeter were performed between 800 and 1400°C on two natural samples: a ugandite from the East African rift and an olivine basalt from the western Mexican arc. Our measurements provide the first in-situ quantitative assessment of enthalpy during melting of initially crystalline natural samples. The distribution of latent heat across the liquidus-solidus intervals of the two samples is distinctly different, reflecting significant variation in the sequence and abundance of mineral phases during melting (clinopyroxene and leucite in the ugandite; olivine, clinopyroxene, and plagioclase in the basalt). Our data further indicate that the common assumption of a uniform distribution of latent heat across the liquidus-solidus interval of a magma is a reasonable approximation for the olivine basalt, but is grossly in error for the ugandite. This is due to cotectic precipitation of leucite and clinopyroxene, leading to a large, disproportionate release of latent heat early in the crystallization sequence. The implication for the thermal history of a crystallizing ugandite magma is that the *rate* of heat loss during conductive cooling will initially be more rapid than the average rate. The net result will be to produce lower magmatic temperatures after a given cooling interval relative to models assuming a uniform release of latent heat. An additional series of scanning calorimetric experiments were performed at variable rates (1, 2, and 3°/min) to evaluate the role of kinetics on the distribution of enthalpy during both melting and crystallization of the ugandite and olivine basalt. The results indicate that clinopyroxene is the most important mineral phase in controlling the shapes of the enthalpy profiles during cooling; this is due to its large enthalpy of fusion and its tendency for sluggish nucleation, followed by rapid crystallization at temperatures that vary with cooling rate. The resolution of the calorimeter (in terms of heat detected per unit time) is also important in determining the shapes of the *observed* enthalpy profiles during these rapid scans. Estimates based on the observed calorimetric signal associated with melting of olivine, and the lack of a calorimetric signal during melting of leucite, combined with known enthalpies of fusion for the two phases, indicate detection limits of approximately 0.6–1.2 kJ per 5 min increments.

R.A. Lange (✉)
Department of Geological Sciences, University of Michigan, Ann Arbor, MI 48109, USA

K.V. Cashman
Department of Geological Sciences, University of Oregon, Eugene, OR 97403, USA

A. Navrotsky
Department of Geological and Geophysical Sciences, Princeton University, Princeton, NJ 08544, USA

Editorial responsibility: T.L. Grove

Introduction

The contribution of latent heat to the thermal evolution of crystallizing magma bodies has been the subject of numerous studies (Lovering 1936; Larsen 1945; Jaeger 1959, 1961; Brandeis et al. 1984; Spohn et al. 1988; Delaney 1988; DeYoreo et al. 1989; Ghiorso 1991; Cashman 1993). In general, the thermal history of a cooling magma body is controlled by a balance between the rate of heat loss to the surrounding country rocks, the heat capacity of the partially molten region, and the production of latent heat associated with crystallization. A significant uncertainty in modelling heat transfer in crystallizing magma bodies arises from deciding how best to model the latent heat term; it enters the differential equation of heat flow as a source term (Carslaw and Jaeger 1959), and therefore must be known a priori as a function of both distance and time.

Solution to this problem has generally involved one of two assumptions: (a) latent heat is released from a magma at a single crystallization temperature, or (b) the total amount of heat released is averaged uniformly over the crystallization interval. The first assumption is wrong, and the second is an over-simplification. Not

only does crystallization in a magma proceed over a large liquidus-solidus interval (typically 250–350°C), but the sequence of crystallization can also vary dramatically between magma types, leading to a non-uniform liberation of latent heat that is unique for each magma. For example, when and if the crystallization path of a magma reaches a two- or three-phase cotectic, there will be a disproportionately large release of heat relative to a comparable cooling interval where only one phase is crystallizing. This effect has been quantitatively demonstrated by Ghiorso (1991) using a thermodynamic solution model (Ghiorso et al. 1983) to calculate the equilibrium crystallization path and enthalpy release for two different magma types: a tholeiite and a boninite. In that study, it was shown that the heat outputs accompanying equilibrium crystallization of the two magma types are quite distinct and are not uniform functions of magmatic temperature.

Documenting enthalpy variations across the liquidus-solidus interval is important not only for studies of crystallization, but also for studies of melt generation in both crustal and mantle source regions. For example, DeYoreo et al. (1989) suggested that the volume of crustal melt produced following a tectonic thickening event can vary by more than a factor of two when the distribution of latent heat over the melting range is changed from linear to quadratic.

Currently, all our information on the release (or absorption) of enthalpy in crystallizing (or melting) magmatic systems is derived from heat of fusion measurements on various pure, end-member mineral components (e.g., $CaMgSi_2O_6$, $NaAlSi_3O_8$, $NaAlSiO_4$, $CaAl_2Si_2O_8$, $CaSiO_3$, $Mg_3Al_2Si_3O_{12}$; Stebbins et al. 1983; Richet and Bottinga 1984). In this paper, we provide the first direct measurements of enthalpy during both melting and crystallization in a natural multicomponent system, specifically a ugandite and an olivine basalt. Our measurements were obtained using a Setaram HT1500 calorimeter in step-scanning mode (Lange and Navrotsky 1992); this approach involves measuring the change in enthalpy of a sample during heating (or cooling) over a small temperature interval (10°C). Two types of experiments are reported: (a) quantitative measurements of "apparent" heat capacity during melting of initially crystalline samples of a ugandite and an olivine basalt, and (b) qualitative enthalpy profiles during both melting and crystallization of a ugandite and an olivine basalt over a range of cooling and heating rates. The latter experiments are used to evaluate the effect of both composition and kinetics on the non-uniform distribution of enthalpy across the liquidus-solidus interval.

Experimental methods

Two samples were chosen for this investigation, an olivine basalt (LV-134, western Mexican volcanic arc; Carmichael et al. unpublished work) and a ugandite (U-150, east African rift, western Uganda; Brown 1971); their compositions are presented in Table 1. These samples were chosen because they have low viscosities, which reduces problems with kinetic delays in melting and crystallization. Moreover, each rock is characterized by a completely different phenocryst assemblage; clinopyroxene and leucite are the dominant phases in the ugandite, whereas olivine, clinopyroxene, and feldspar occur in the olivine basalt.

Table 1 Electron microprobe analyses (wt%) of quenched glassy samples

Sample:	Ugandite	Olivine Basalt
SiO_2	40.24	48.83
TiO_2	4.83	1.19
Al_2O_3	8.24	12.04
Fe_2O_3	9.51	5.77
FeO	2.90	2.51
MnO	0.22	0.18
MgO	9.72	16.69
CaO	14.26	7.36
Na_2O	1.18	2.42
K_2O	6.57	1.93
P_2O_5	1.52	0.54
Total	99.19	99.46

[a] Ferric-ferrous ratio calculated from Kilinc et al. (1983) assuming equilibrium in air at 1400°C

Before calorimetry, each sample was pre-loaded into a 95% Pt-5% Au capsule and fused overnight in a box furnace in air above its liquidus. The capsule was then cleaned with HF and a fresh batch of sample was re-loaded into the same Pt-Au capsule. This presaturation procedure, combined with the fact that the calorimetric measurements were performed in air, minimized iron loss from the sample to the capsule.

Calorimetric measurements were made with a Setaram HT-1500 calorimeter in both step-scanning mode (for quantitative measurements of apparent heat capacity) and scanning mode (for qualitative "instantaneous" enthalpy profiles). Because the apparatus and experimental procedure have been described in detail by Lange et al. (1991) and Lange and Navrotsky (1992), only a brief summary is presented here. The calorimetric detector consists of an upper and lower thermopile surrounding a sample and reference chamber respectively. Approximately 1 g of sample was held in a 95% Pt-5% Au crucible that was contained within the sample chamber in air. During a step-scanning run, the thermopile voltage was monitored as the temperature was raised at a rate of 1°C/min over 10°C. A 10 min heating period was followed by a 15 min isothermal interval to allow thermal equilibration (and the voltage to return to baseline). A typical run consisted of ten heating steps. The integrated area under each voltage peak represents one datum point. A single, step-scanning experiment consisted of three runs: a blank (empty Pt crucible), a calibration (corundum powder), and a sample. The results of the blank were subtracted from those of the calibration and sample runs, and the corundum C_p data of Robie et al. (1978) were used to derive C_p values for the samples. A detailed discussion of the precision and accuracy of these experiments is found in Lange and Navrotsky (1992). The standard deviations on the average integrated areas for the blank, calibration, and sample runs lead to a propagated error on C_p(sample) of 5–10%.

Experiments were also conducted in scanning mode. In this approach, the voltage difference between the sample and reference thermopiles was monitored as a sample was cooled (crystallized) or heated (melted) at a constant rate (one, two, and three °C/min in different experiments). The calorimetric signal recorded across the liquidus-solidus interval of each sample is directly proportional to the instantaneous enthalpy release or absorption during crystallization and melting, respectively.

Cooling and heating quench experiments. Simulations of each calorimetric experiment were performed in a quench vertical tube

furnace. Samples were run through the same thermal history as experienced in the calorimeter, and quenched at various temperatures corresponding to "key" regions observed in the calorimetric experiments. This was necessary because actual calorimetric runs cannot be quenched but cool over several hours before disassembly. The quenched samples were cut in half and mounted in epoxy for electron microprobe analyses and back-scattered electron (BSE) images. Analyses of the quenched charges were performed using a Cameca Camebax electron microprobe; standard operating conditions consisted of a focused electron beam, an accelerating current of 15 kV, and a sample current of 10 nA. Backscattered electron images were obtained with a Hitachi S-570 scanning electron microscope at the University of Michigan and a JEOL 6300 scanning electron microscope at the University of Oregon. Measurement of sample modes was performed by digital image analysis of BSE images using Dapple "Prism" software. On samples where the gray scale contrast of individual phases was insufficient to differentiate between them, modes were measured based on single x-ray element maps; discrimination of phases was performed using Link software.

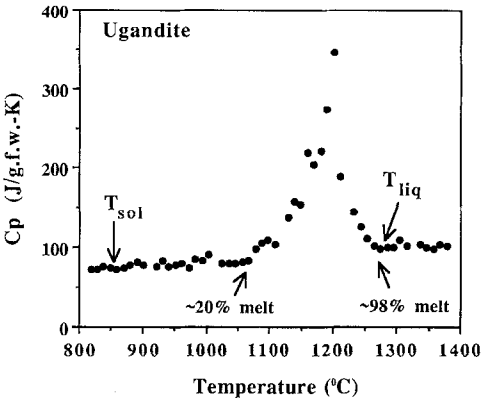

Fig. 1 Plot of measured heat capacity vs temperature during melting of the ugandite. T_{sol} and T_{liq} refer to the solidus and liquidus temperaures respectively

In-situ measurements of latent heat during melting

Quantitative measurements of "apparent" heat capacity (the absorption of latent heat over 10°C increments):

$$\frac{H_{T+\Delta T} - H_T}{\Delta T} = C_p^{apparent} = \frac{\Delta H_{fusion}}{\Delta T} + C_p \qquad (1)$$

were made during melting of the initially crystalline ugandite sample and olivine basalt sample. The powdered rocks were initially taken to temperatures above their liquidi (1300°C and 1400°C respectively), then cooled slowly (5°/h) to 800°C, and held there for 24 h prior to the first calorimetric step-scanning run. The same heating and cooling sequences were also performed on each rock in a vertical tube quench furnace; samples were quenched at 800°C in order to determine their modes at the beginning of their respective melting calorimetric runs.

Ugandite

The fully crystalline ugandite sample has a modal composition of approximately 25% leucite, 45% clinopyroxene, 16% titanomagnetite, 7% perovksite, 4% nepheline, and 3% olivine at 800°C. Calorimetric measurements were collected between 818 and 1378°C; heat capacities (based on the change in enthalpy over each 10°C interval) are reported in Table 2 and Fig. 1. The most striking feature is the abrupt rise in heat capacity that begins at approximately 1050°C, peaks at 1200°C, and then falls to a relatively constant value at ~1250°C. Simulation melting experiments in a quench furnace indicate that at 1050°C there is ~20% melt, and leucite, clinopyroxene, olivine, and spinel are the only remaining phases. Resorption textures further show that the abrupt rise in heat capacity at ~1050°C corresponds to the onset of melting of clinopyroxene; this is followed by significant melting of leucite by ~1160°C. Clinopyroxene is completely melted by 1220°C, leucite is gone by 1250°C, and olivine and titanomagnetite persist until 1267°C. The small peak at ~1310°C appears to be an artifact (reflecting the scatter in the data at high temperature) since quenched melting runs have only pure glass between 1270 and 1310°C.

Figure 1 shows that the C_p curve can resolve the liquidus temperature of the ugandite sample, although definition of the solidus is less clear. This is because the melt fraction across the liquidus-solidus curve is not linear. For example, only ~20% of the rock melts during the first 200°C of the solidus-liquidus interval (850–1050°C), whereas more than 75% melts over the next 200°C (1050–1250°C). The region close to the liquidus is, therefore, much more readily resolved than the solidus by calorimetry.

The distribution of enthalpy across the liquidus-solidus interval was calculated by integration of the heat capacity curve in Fig. 1 using the following relationship:

$$H_T - H_{Ti} = \int_{Ti}^{T} C_p(T)\, dT \qquad (2)$$

where T_i is the initial temperature of measurement and T is the experimental temperature. Area integration was performed by cubic interpolation of the data points with the stipulation that at 1200°C, the C_p reaches a maximum. Although the enthalpy of the crystalline sample at T_i (807°C) relative to its standard state enthalpy at 25°C is not known (i.e., $H_{807} - H_{25°C}$), the difference in relative enthalpy between the solidus and liquidus temperatures can be readily computed. Values of $H_T - H_{Ti}$ for the ugandite sample are listed in Table 2. The total enthalpy of fusion is 49 kJ/gfw[1] for the multiphase rock.

Olivine basalt

The distribution of latent heat during melting of the olivine basalt sample is distinctly different from that for

[1] gfw = gram fromula weight $= \Sigma X_i MW_i$, where X_i is the mole fraction of each oxide component and MW_i is the molecular weight of each oxide component

Table 2 Ugandite heat capacity and enthalpy data

Temp K	Cp J/gfw-K (meas)	Cp J/gfw-K (calc)[a]	Δ J/gfw-K	H_T-H_{Ts} kJ/gfw (meas)	H_T-H_{Ts} kJ/gfw (calc)[a]	Δ kJ/gfw
807				0	0	0
818	72.7	72.7	0	0.8	0.8	0
828	72.5	72.5	0	1.5	1.5	0
838	75.5	75.5	0	2.3	2.3	0
849	74.8	74.8	0	3.1	3.1	0
859	72.1	72.1	0	3.8	3.8	0
870	74.4	120.8	−46.4	4.6	5.2	−0.6
880	78.0	120.8	−42.8	5.4	6.4	−1.0
890	81.8	120.8	−39.0	6.2	7.6	−1.4
901	78.0	120.8	−42.8	7.1	8.9	−1.8
921	76.0	120.8	−44.8	8.6	11.3	−2.7
931	83.3	120.8	−37.5	9.5	12.5	−3.0
941	75.4	120.8	−45.4	10.2	13.7	−3.5
952	78.3	120.8	−42.5	11.1	15.1	−4.0
962	79.4	120.8	−41.4	11.9	16.3	−4.4
973	74.0	120.8	−46.8	12.7	17.6	−4.9
983	85.3	120.8	−35.5	13.5	18.8	−5.3
993	82.8	120.8	−38.0	14.4	20.0	−5.6
1004	90.8	120.8	−30.0	15.4	21.3	−5.9
1025	80.0	120.8	−40.8	17.0	23.9	−6.9
1035	79.8	120.8	−41.2	17.8	25.1	−7.3
1045	79.2	120.8	−41.6	18.6	26.3	−7.7
1056	81.0	120.8	−39.8	19.5	27.6	−8.1
1066	84.0	120.8	−36.8	20.4	28.8	−8.4
1077	98.4	120.8	−22.4	21.4	30.2	−8.8
1087	105.9	120.8	−14.9	22.5	31.4	−8.9
1097	110.5	120.8	−10.3	23.6	32.6	−9.0
1108	104.2	120.8	−16.6	24.7	33.9	−9.2
1129	137.8	120.8	17.0	27.6	36.4	−8.8
1139	158.9	120.8	38.1	29.2	37.6	−8.4
1149	155.1	120.8	34.3	30.8	38.9	−8.1
1160	218.8	120.8	98.0	33.2	40.2	−7.0
1170	205.5	120.8	84.7	35.2	41.4	−6.2
1181	222.2	120.8	101.4	37.7	42.7	−5.0
1191	273.4	120.8	152.6	40.4	43.9	−3.5
1201	346.2	120.8	225.4	43.9	45.1	−1.2
1212	189.5	120.8	68.7	46.0	46.5	−0.5
1233	145.4	120.8	24.6	49.0	49.0	0.0
1243	126.6	120.8	5.8	50.3	50.2	0.1
1253	111.2	120.8	−9.6	51.4	51.4	0.0
1264	101.5	101.5	0	52.5	52.5	0.0
1274	98.9	98.9	0	53.5	53.5	0.0
1285	101.0	101.0	0	54.6	54.6	0.0
1295	100.6	100.6	0	55.6	55.6	0.0
1305	110.6	110.6	0	56.7	56.7	0.0
1316	101.9	101.9	0	57.8	57.8	0.0
1336	103.6	103.6	0	59.9	59.9	0.0
1347	100.4	100.4	0	61.0	61.0	0.0
1357	98.2	98.2	0	62.0	62.0	0.0
1368	104.6	104.6	0	63.2	63.2	0.0
1378	102.1	102.1	0	64.2	64.2	0.0

[a] Based on the assumption of a uniform distribution of latent heat

the ugandite sample. The fully crystalline olivine basalt has a modal composition of approximately 26% olivine, 32% plagioclase, 19% clinopyroxene, 12% titanomagnetite, and 9% alkali feldspar at 900°C. Calorimetric measurements were collected between 820 and 1422°C; heat capacities are reported in Table 3 and Fig. 2. In contrast to the ugandite C_p profile, the most striking feature in Fig. 2 is the lack of a well-defined peak at the liquidus temperature. From quenched melting experiments undergoing the same thermal history as in the calorimetric run, it is clear that ~85% of the rock has melted by 1260°C, yet olivine and spinel do not disappear until 1343°C. In contrast to the ugandite, the last 15% of melting occurs over 80°C. There is only a subtle reflection of this feature in the calorimetric curve. In contrast, the solidus is fairly well marked by the bump in the calorimetric curve that begins at ~935°C and marks the initial melting of alkali feldspar. The more significant rise in the C_p curve, which begins at ~1050°C and peaks at ~1170°C, corresponds to the melting of both plagioclase and clinopyroxene, which are completely gone by 1200°C. Quench melting experi-

Table 3 Olivine basalt heat capacity and enthalpy data

Temp K	Cp J/gfw-K (meas)	Cp J/gfw-K (calc)[a]	Δ J/gfw-K	H_T-H_{Ts} kJ/gfw (meas)	H_T-H_{Ts} kJ/gfw (calc)[a]	Δ kJ/gfw
810	–	–	–	0	0	0
820	81.4	81.4	0	0.8	0.8	0
830	78.7	78.7	0	1.6	1.6	0
840	82.3	82.3	0	2.4	2.4	0
851	84.1	84.1	0	3.3	3.3	0
861	78.5	78.5	0	4.1	4.1	0
872	81.8	81.8	0	5.0	5.0	0
882	82.1	82.1	0	5.9	5.9	0
892	86.7	86.7	0	6.7	6.7	0
903	85.4	85.4	0	7.7	7.7	0
924	85.6	85.6	0	9.5	9.5	0
934	94.3	94.3	0	10.4	10.4	0
944	95.8	95.8	0	11.4	11.4	0
955	93.1	93.1	0	12.4	12.4	0
965	98.9	112.0	−13.1	13.4	13.5	−0.1
976	91.5	112.0	−20.5	14.4	14.7	−0.4
986	84.9	112.0	−27.1	15.2	15.9	−0.6
996	96.5	112.0	−15.5	16.2	17.0	−0.8
1007	95.7	112.0	−16.3	17.2	18.2	−1.0
1028	102.9	112.0	−9.1	19.4	20.6	−1.2
1038	99.7	112.0	−12.3	20.4	21.7	−1.3
1048	92.5	112.0	−19.5	21.3	22.8	−1.5
1059	100.6	112.0	−11.4	22.4	24.0	−1.6
1069	96.1	112.0	−15.9	23.4	25.2	−1.8
1080	112.0	112.0	0	24.6	26.4	−1.8
1090	110.8	112.0	−1.2	25.7	27.5	−1.8
1100	117.7	112.0	5.7	26.9	28.6	−1.7
1111	104.8	112.0	−7.2	28.1	29.9	−1.8
1133	134.4	112.0	22.4	31.0	32.3	−1.3
1143	140.5	112.0	28.5	32.4	33.4	−1.0
1153	155.9	112.0	43.9	34.0	34.6	−0.6
1164	153.6	112.0	41.6	35.7	35.8	−0.1
1174	159.1	112.0	47.1	37.3	36.9	+0.4
1185	135.3	112.0	23.3	38.8	38.1	+0.6
1195	106.0	112.0	−6.0	39.8	39.3	+0.6
1205	114.1	112.0	2.1	41.0	40.4	+0.6
1216	118.1	112.0	6.1	42.3	41.6	+0.6
1236	112.8	112.0	0.8	44.5	43.9	+0.7
1247	111.8	112.0	−0.2	45.7	45.1	+0.7
1257	118.9	112.0	6.9	46.9	46.2	+0.7
1268	96.8	112.0	−15.2	48.0	47.4	+0.6
1278	100.8	112.0	−11.2	49.0	48.6	+0.4
1288	100.5	112.0	−11.5	50.0	49.7	+0.3
1299	112.3	112.0	0.3	51.2	50.9	+0.3
1309	101.7	112.0	−10.3	52.3	52.0	+0.2
1319	103.6	112.0	−8.4	53.3	53.2	+0.1
1339	104.2	112.0	−7.8	55.4	55.4	0
1350	98.4	98.4	0	56.5	56.5	0
1360	102.3	102.3	0	57.5	57.5	0
1371	105.1	105.1	0	58.7	58.7	0
1381	99.9	99.9	0	59.7	59.7	0
1391	102.6	102.6	0	60.7	60.7	0
1402	100.9	100.9	0	61.8	61.8	0
1412	101.6	101.6	0	62.8	62.8	0
1422	100.2	100.2	0	63.8	63.8	0

[a] Based on the assumption of a uniform distribution of latent heat

ments further indicate that by 1050°C, ~30% of the rock is melted and over the next 160°C (1050–1210°C) an additional 50% of the rock melts. This latter pulse of melting is easily resolved by the calorimetric measurements. Again, the melt fraction across the liquidus-solidus interval is far from linear.

The distribution of enthalpy across the liquidus-solidus interval for the olivine basalt was calculated by integration of the heat capacity curve in Fig. 2 using the relationship in Eq. 1. Again, area integration was performed by cubic interpolation of the data points with the stipulation that at 1170°C, the C_p reaches a maximum. Values of H_T–H_{Ti} for the olivine basalt are listed in Table 3. The total enthalpy of fusion is 43 kJ/gfw for the initially crystalline rock.

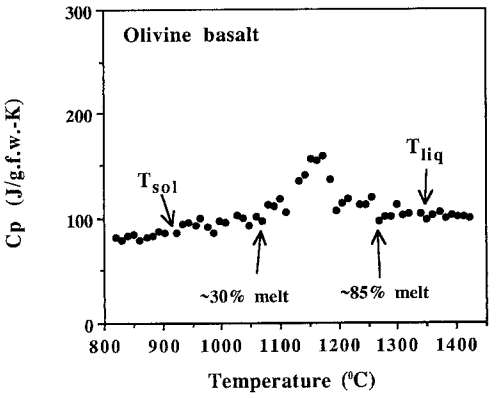

Fig. 2 Plot of measured heat capacity vs temperature during melting of the basalt. T_{sol} and T_{liq} refer to the solidus and liquidus temperaures respectively

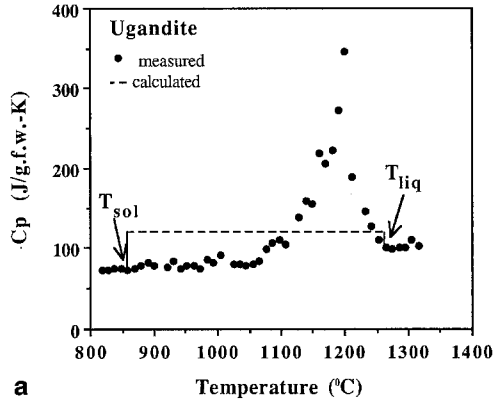

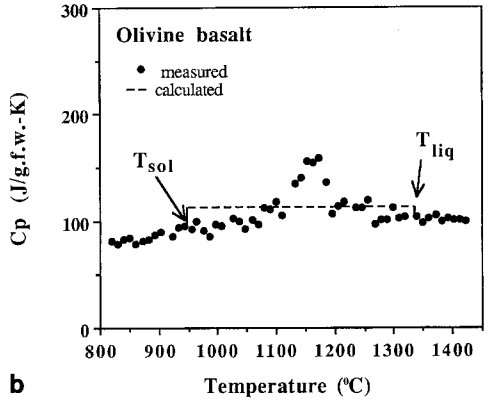

Fig. 3a,b Comparison of the measured heat capacity curves during melting of **a** the ugandite and **b** the basalt with those calculated (*dashed curves*) assuming a uniform distribution of latent heat. By defintion, integrations of the measured and calculated heat capacity curves lead to the same enthalpy of fusion for each sample

How good is the assumption of a uniform distribution of latent heat?

We can now compare our in-situ measurements of latent heat during melting of the ugandite and olivine basalt samples with the common assumption that latent heat is

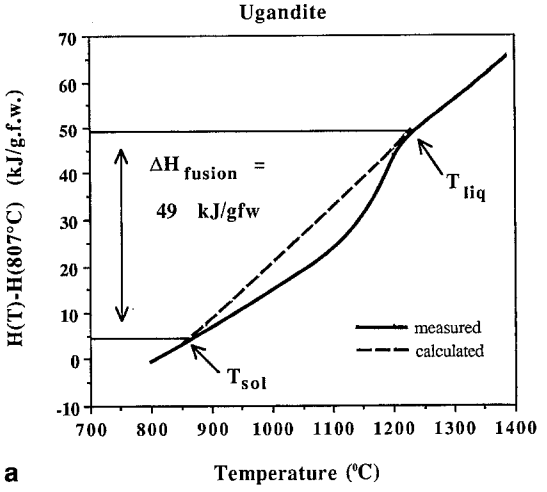

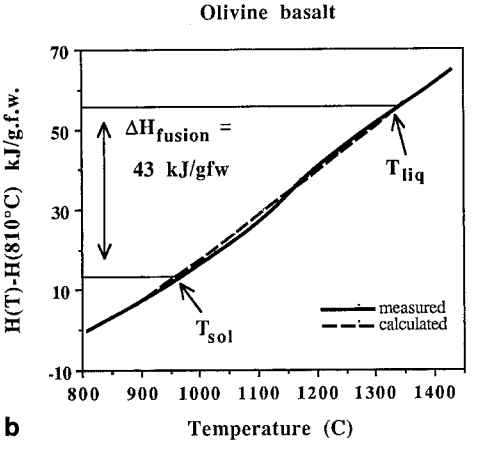

Fig. 4a, b Comparison of a calculated "uniform" distribution of enthalpy (*dashed curve*) with that obtained by in-situ measurements (*solid curve*) for **a** the ugandite and **b** the olivine basalt

distributed uniformly across the liquidus-solidus interval. We calculated the area under the measured C_p curves in Figs. 1 and 2 and then redistributed the same area uniformly between the solidus and liquidus of each sample, as seen in Fig. 3a and 3b. The calculated C_p value across the liquidus-solidus interval for each sample is listed in Tables 2 and 3 for comparison to the measured values. Integration of the "uniform" C_p curves was performed using the relation in Eq. 1; the "uniform" distribution of enthalpy is compared with that obtained from our in-situ measurements in Tables 2 and 3 and Fig. 4a,b. By definition, integration of the "uniform" C_p curve leads to the same total enthalpy of fusion between the solidus and liquidus for each sample. What is different, however, is the *rate* at which heat is absorbed (or released) during melting (or crystallization) as a function of temperature. We can now use the measured and calculated distributions of enthalpy for each sample to infer cooling histories.

For example, examination of the in-situ enthalpy measurements on the ugandite sample (Fig. 4a) indicates that latent heat will be released at a faster *rate*per

increment drop in temperature relative to a model in which latent heat is distributed uniformly across the crystallization interval. This is caused by cotectic precipitation of leucite and clinopyroxene, leading to a large, disproportionate release of latent heat early in the crystallization sequence. This requires that the rate of heat loss during conductive cooling of this ugandite magma will initially be more rapid than the average rate. The net result will be to produce lower magmatic temperatures after a given cooling interval, relative to models assuming a uniform release of latent heat.

Ghiorso (1991) observed the same phenomenon when modelling the conductive cooling path of an olivine tholeiite from Thingmuli, Iceland. In that study, Ghiorso's thermodynamic model (Ghiorso et al. 1983) was used to show that olivine, plagioclase, and clinopyroxene all crystallize within 30°C of the liquidus temperature. Just as in the case of the ugandite magma, there is a disproportionately large release of latent heat accompanying this cotectic precipitation that occurs early in the crystallization interval. Ghiorso (1991) further showed that the assumption of a uniform distribution of heat leads to an overestimation of the magmatic temperature (during conductive cooling of a 1000 km^3 olivine tholeiite magma body) by as much 60°C after 500,000 years of cooling, and ~100°C after 700,000 years of cooling. In other words, the crustal residence time of a cooling olivine tholeiitic magma body will be overestimated. Similar conclusions can be drawn regarding the cooling history of the ugandite magma body or *any* magma which crystallizes a large proportion of phases (i.e., reaches a cotectic) early in its crystallization sequence.

The distribution of latent heat across the liquidus-solidus interval of the olivine basalt is in direct contrast to this behavior. Unlike the ugandite, the olivine basalt undergoes a protracted crystallization sequence in which olivine is the dominant precipitating phase for over 200°C before the system reaches a cotectic, first with clinopyroxene and then with plagioclase. Although there is a large release of latent heat at this point, the important aspect is that it occurs approximately in the middle of the liquidus-solidus interval. In Fig. 4b, the distribution of enthalpy derived assuming a uniform release of latent heat is very similar to that derived from our in-situ measurements. In other words, the approximation of a uniform distribution of latent heat is quite good for the olivine basalt sample. This behavior is similar to that calculated by Ghiorso (1991) for a boninite magma. In that study, Ghiorso's thermodynamic model was used to demonstrate that a boninite magma also undergoes a long crystallization sequence in which orthopyroxene is the only precipitating phase for over 200°C until it finally reaches a cotectic with plagioclase. Again, the large pulse of released latent heat occurs approximately midway through a long, protracted liquidus-solidus interval. The conductive cooling model of Ghiorso (1991) demonstrates that the approximation of a uniform distribution of latent heat is a good one for the boninite, primarily because the large heat release at the cotectic occurs in the middle of the crystallization sequence.

A corollary to these observations is that a magma undergoing signficant crystallization at temperatures very close to the solidus (e.g., crustal melts under water-saturated conditions; see Wyllie 1977; Wickham 1987) will not be well approximated as having a uniform distribution of latent heat. For such magmas, there will be a disproportionate release of latent heat late in the crystallization sequence. In this case, the rate of heat loss during conductive cooling will initially (near the liquidus) be slower than the average rate. The net result will be to predict higher magmatic temperatures after a given cooling interval relative to models assuming a uniform release of latent heat. In other words, the crustal residence time for such a cooling magma body will be underestimated.

Enthalpy profiles during melting and crystallization as a function of cooling and heating rates

An additional series of scanning calorimetric experiments were performed to evaluate the role of kinetics on the distribution of enthalpy during melting and crystallization. During these runs, the thermopile voltage was monitored as each sample was cooled and heated at a given rate (1, 2 and 3°/min). The calorimetric signal is directly proportional to the "instantaneous" release or absorption of latent heat during crystallization and melting, respectively. These experiments demonstrate that a variation in cooling and heating rate can give rise to dramatically different enthalpy profiles (Fig. 5).

Another goal of the scanning experiments was to determine the minimum heat content per unit time that can be resolved by the calorimeter during these rapid scans. A series of BSE photographs (Figs. 6, 7) were taken of both the olivine basalt and ugandite samples quenched from simulated heating and cooling experiments at two different rates: 3° and 1°/min. Quench temperatures closely correspond to the beginning, peak, and final temperatures over which a heat effect could be resolved from the respective calorimetric curves in Fig. 5. Tables 4 and 5 list the modes for each sample, allowing correlation of mineral abundance to "key" regions along the calorimetric curves. Quantification of the modes allows constraints to be placed on the minimum extent of crystallization (or melting) of various mineral phases that can be detected. In other words, it is possible to determine how much of each phase per unit time must be crystallizing (or melting) in order to be resolved by the calorimetric signal.

Olivine basalt: heating and cooling scans

The results of heating and cooling scans at variable rates (1, 2, and 3°/min) for the olivine basalt are present-

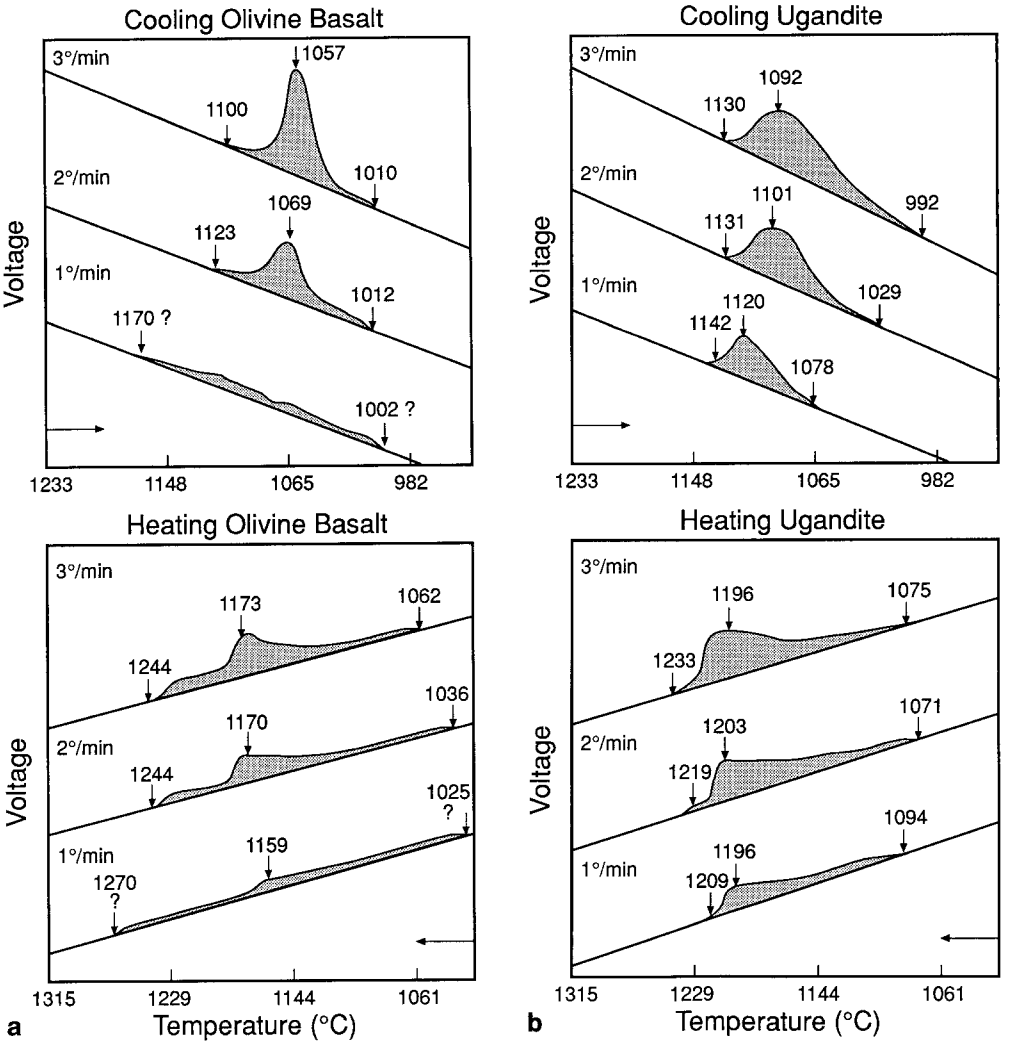

Fig. 5 **a** The results of a series of crystallization and melting experiments on the olivine basalt in the calorimeter at constant cooling and heating rates of 3°, 2°, and 1°/min. **b** The results of a series of crystallization and melting experiments on the ugandite in the calorimeter at constant cooling and heating rates of 3°, 2°, and 1°/min

ed in Fig. 5a. Prior to each run, the samples were taken to 1300°C, held for six hours, and then cooled slowly (5°/h) to 800°C. For the heating runs, the experiments then began at 800°C.

In Fig. 5a, it can be seen that the temperature interval over which a heat effect can be resolved for the olivine basalt is a function of both (1) whether the sample is being heated or cooled and (2) the scanning rate. For relatively rapid (3°/min) heating and cooling scans, the heat effect is resolved over intervals of 186 and 90°C, respectively. The highest temperature for which a heat effect can be resolved is 1248°C for the heating scan and 1100°C for the cooling scan. The modal data (Table 4) show that the upper temperature limits correspond to melt fractions of 0.96 at 1248°C during heating and 0.89 at 1100°C during cooling. The difference between the two melt fractions is small (.07), given the estimated error in the modes ($\pm$.05). Therefore, the large difference in the upper limit temperatures (1248 and 1100°C) primarily reflects the kinetic suppression of nucleation and crystallization during rapid cooling compared to kinetic hindrances to melting during heating. There is very little difference in the lower temperature limits (for which a heat effect can be resolved) between the rapid heating and cooling scans (1062 and 1025°C, respectively); both lower temperatures correspond to a melt fraction of 0.72 (Table 4).

For the slower heating and cooling scans (1°/min), the latent heat effect is resolved over larger temperature intervals relative to the faster scans (3°/min). During heating, the temperature interval is 235°C at 1°/min (vs 186°C at 3°/min), whereas during cooling, the interval is 168 (vs 90)°C. The highest temperature for which a heat effect can be resolved is ~1270°C for the heating scan and ~1170°C for the cooling scan; both upper limit temperatures correspond to a melt fraction of ~0.92. Again, the difference in the upper limit temperatures (1270 vs 1170°C) can be attributed to kinetic delays in nucleation during cooling. As observed for the rapid scans, there is not much difference in the lower temperature limits (1025 and 1002°C, respectively) between the heating and cooling scans at 1°/min; both temperatures correspond to melt fractions of 0.68 (Table 4).

The most striking feature of the basalt heating and cooling scans at both 3° and 1°/min is that the latent heat profiles only reflect ~20–30% melting and crystal-

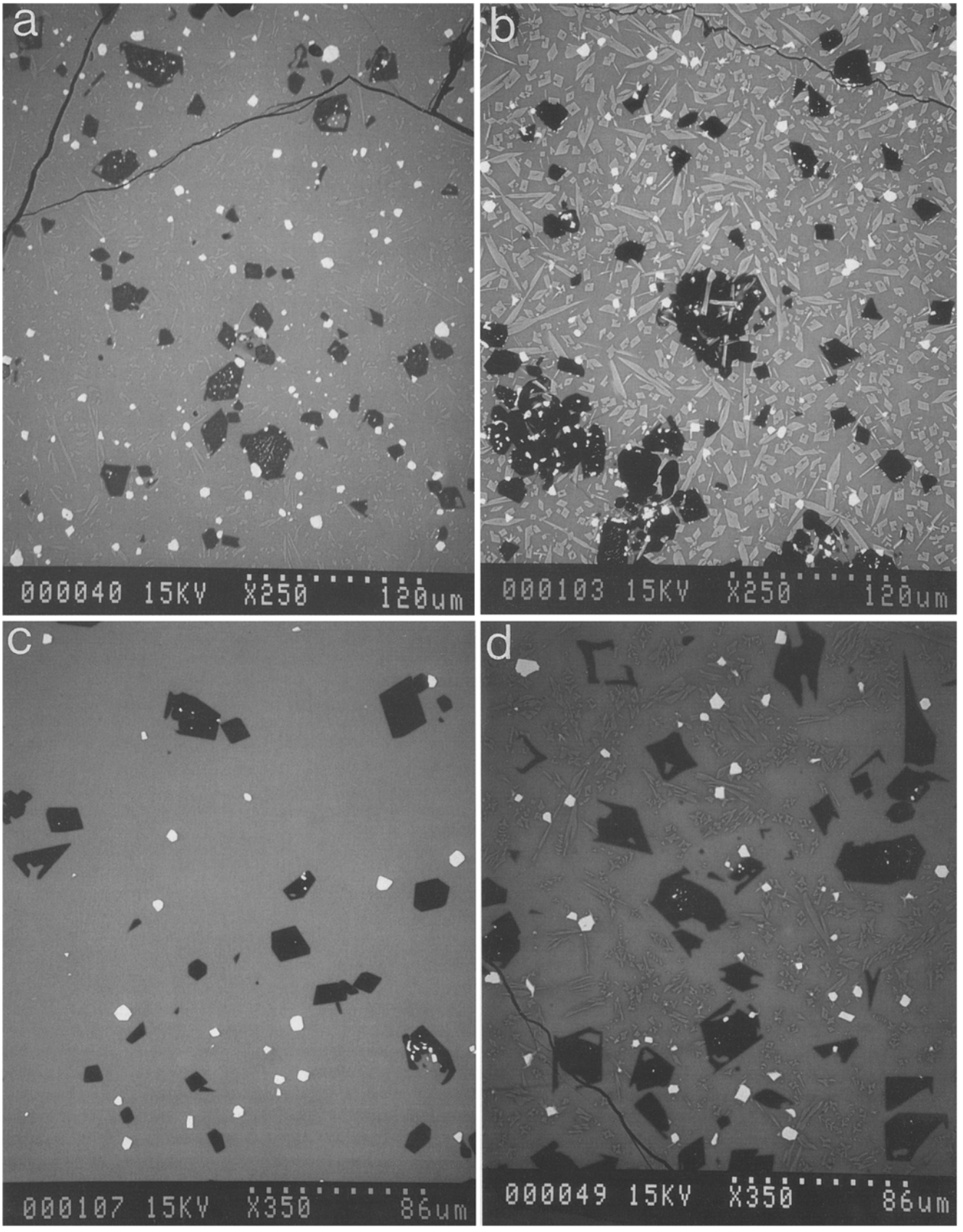

Fig. 6a–d Representative BSE images of the olivine basalt sample, **a** quenched at 1144°C from a heating (3°/min) run, **b** quenched at 1025°C from a heating (1°/min) run, **c** quenched at 1170°C from a cooling (1°/min) run **d** quenched at 1057°C from a cooling (3°/min) run. In order from darkest to lightest, the phases are olivine, glass, clinopyroxene, and spinel

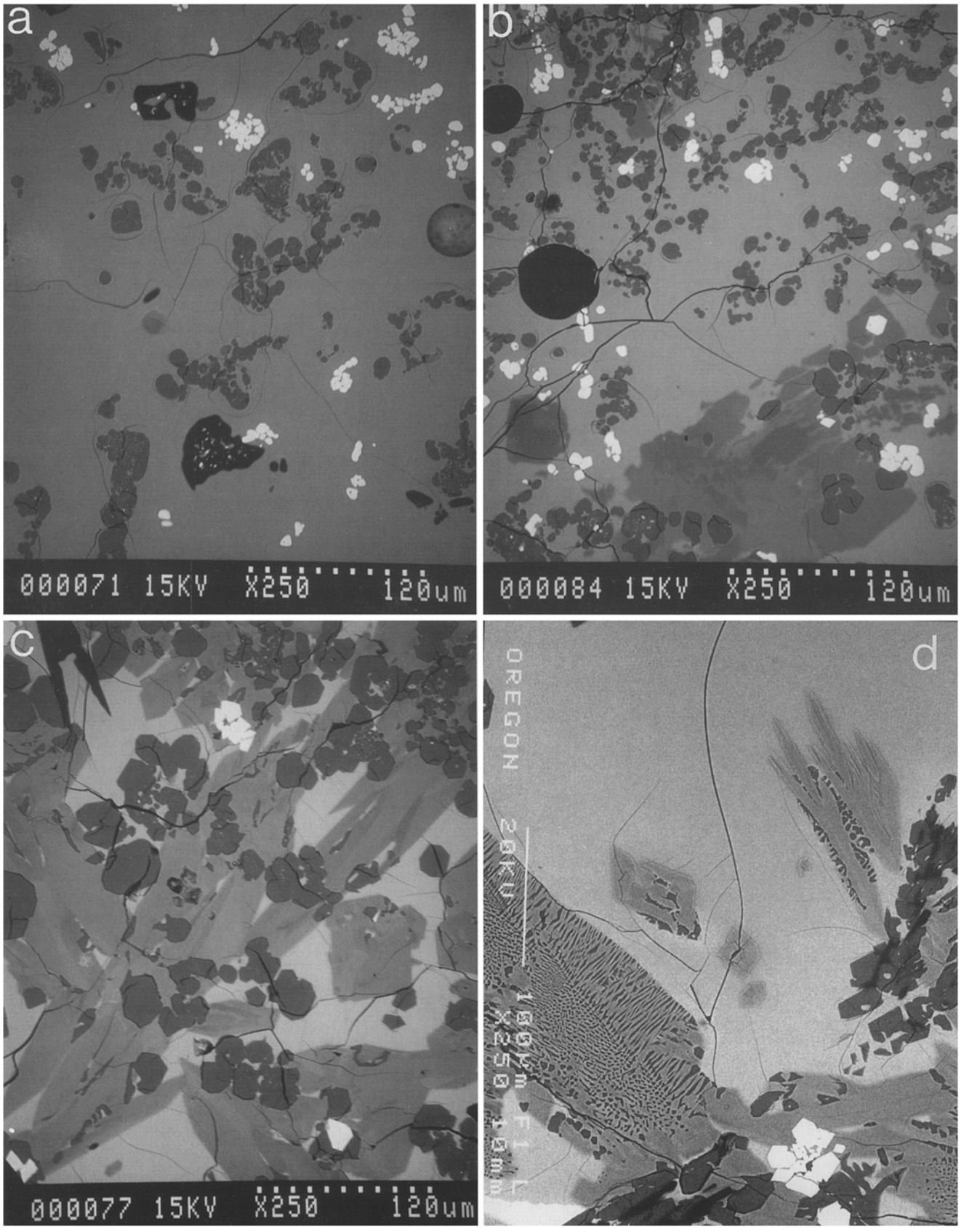

Fig. 7a–d Representative BSE images of the ugandite sample, **a** quenched at 1232°C from a heating (3°/min) run, **b** quenched at 1209°C from a heating (1°/min) run, **c** quenched at 1095°C from a cooling (3°/min) run, **d** quenched at 1142°C from a cooling (1°/min) run. In order from darkest to lightest, the phases are olivine, leucite, clinopyroxene, glass, and spinel

Table 4 Modal % of mineral phases during basalt scans

3°/min: heating			
Temperature	1248°C	1200°C	1062°C?
Glass	96	91	72
Spinel	<1	<1	1
Clinopyroxene'	–	–	14
Olivine	4	8	13
3°/minute: cooling			
Temperature	1100°C	1057°C	1010°C
Glass	89	80	72
Spinel	1	1	2
Clinopyroxene'	–	14	19
Olivine	10	5	7
1°/minute: heating			
Temperature	1260°C	1165°C	1025°C
Glass	93	84	68
Spinel	<1	2	2
Clinopyroxene'	–	6	23
Olivine	5	6	8
1°/minute: cooling			
Temperature	1170°C	1078°C	1010°C
Glass	91	77	68
Spinel	<1	2	2
Clinopyroxene'	–	10	30
Olivine	8	8	5

lization. The modes in Table 4 indicate that plagioclase never crystallized during the cooling runs and was never present at the beginning of a heating run. This reflects the sluggish nucleation of feldspar in the basalt liquid. Prior to the heating runs, the olivine basalt was not held at 800°C long enough (only 6 h) to crystallize feldspar. In contrast, prior to the step-scanning run of the olivine basalt (results shown in Fig. 2), the sample was held for 48 h. The presence of crystalline feldspar at the beginning of the step-scanning experiment, in addition to the improved detection limits when running in step-scanning vs scanning mode (see Lange et al. 1991 for detailed discussion), led to the vastly different calorimetric profiles observed during heating of the olivine basalt at 1°/min between Fig. 2 and Fig. 5.

It should also be noted that the sharp peak observed for the olivine basalt sample during the rapid cooling scan (3°/min) corresponds to the onset of clinopyroxene crystallization during cooling (~14% at the peak temperature). In marked contrast, during the slower cooling scan, the effect of clinopyroxene (~10% at 1078°C) is barely detected in the calorimetric signal. Again, the differences between the two profiles (rapid vs slow cooling), can be attributed to how much heat *per unit time* can be resolved with the calorimeter.

Ugandite: heating and cooling scans

The results of heating and cooling scans at variable rates (1, 2, and 3°/min) for the ugandite are presented in Fig. 5b. Prior to each run, the samples were taken to 1300°C, held for 6 h, and then cooled slowly (5°/h) to 800°C. For the heating runs, the experiments then began at 800°C.

Table 5 Modal % of mineral phases during ugandite scans. (In this sample, the distribution of phases was heterogeneous with scattered clots of crystals. Errors are also introduced from the fact that the modes are determined from a two-dimensional cross section through a three-dimensional sample volume)

3°/minute: heating			
Temperature	1232°C	1196°C	1075°C
Glass	86	65	24
Spinel	2	4	3
Clinopyroxene'	–	17	43
Leucite	12	22	31
Olivine	?	3	?
3°/minute: cooling			
Temperature	1130°C	1092°C	992°C
Glass	87	32	17
Spinel	2	2	3
Clinopyroxene'	5	38	47
Leucite	6	22	26
Olivine	?	3	7
1°/minute: heating			
Temperature	1209°C	1192°C*	1096°C
Glass	56	44–53	26
Spinel	2	2–3	10
Clinopyroxene'	12	20–25	25
Leucite	30	19–25	38
Olivine	?	?	?
1°/minute: cooling			
Temperature	1142°C	1120°C	1078°C
Glass	68	31	28
Spinel	4	5	3
Cinopyroxene'	16	31	43
Leucite	12	32	26
Olivine	?	?	?

One of the striking features of the ugandite scans is that the temperature interval over which a heat effect can be resolved appears to *decrease* as both the heating and cooling rates decrease; this is opposite to the trend observed for the basalt. For relatively rapid heating and cooling conditions (3°/min), the heat effect is resolved over 158 and 138°C intervals respectively, whereas for slower heating and cooling conditions (1°/min), the heat effect is resolved over shorter intervals of 115 and 64°C, respectively.

From Table 5, it is clear that in all four cases (rapid and slow heating; rapid and slow cooling), the lowest temperatures for which the heat effect can be detected all correspond to a relatively constant melt fraction of ~0.2–0.3. In contrast, the heating and cooling *rate* determines the extent to which crystallization or melting near the liquidus can be resolved. For example, during rapid (3°/min) heating and cooling, the highest temperatures for which a heat effect is resolved correspond to a constant melt fraction of ~0.9, whereas during slow (1°/min) heating and cooling, the highest temperatures correspond to a melt fraction of ~0.7. This observation is important in terms of the resolution of the calorime-

ter. During the slow cooling scan (1°/min), a full 30% of crystallization occurs near the liquidus that is undetected by the calorimetric signal. Again, this demonstrates the sensitivity of the calorimeter to the heat produced *per unit time*.

The effect of kinetic delays to the nucleation of clinopyroxene is also evident from the ugandite scans at variable cooling rates. For example, the highest temperatures for which a heat effect can be detected are very different between heating and cooling scans performed at the same rate (e.g., 1232 vs 1130°C at 3°/min and 1209 vs 1142°C at 1°/min). As for the olivine basalt, this clearly shows the kinetic suppression of nucleation and crystallization during cooling compared to kinetic hindrances to melting during heating.

An additional important observation that can be drawn from the calorimetric curves relates to the difference in viscosity between the olivine basalt and ugandite liquids. The modal data found in Table 5 indicate that during the rapid scans (3°/min), the ugandite calorimetric curves reflect ~50–60% of crystallization and melting; this is *twice* what is observed for the olivine basalt. This difference is due to the fact that the ugandite melt is significantly more fluid than the olivine basalt melt, allowing leucite to nucleate more readily than plagioclase. Significant crystallization of leucite occurs, therefore, during rapid cooling, and the resulant release of latent heat is observed. Consequently, a significant proportion of leucite (~30–40%) is present in the ugandite sample prior to all heating runs; 6 h at 800°C is clearly sufficient time to allow leucite to crystallize fully in the charge. The contribution from the melting of leucite to the latent heat profile is, therefore, always observed during the heating runs.

Detection limits (kJ/min) of the calorimeter in scanning mode

The minimum amount of heat per unit time that is resolved by the calorimeter can be estimated by calculating how much of any one phase melted or crystallized without detection during various heating or cooling scans. For example, during the 3°/min heating scan of the olivine basalt, the calorimetric signal obtained at temperatures above the peak (signalling the completion of clinopyroxene melting) can be attributed exclusively to the melting of olivine. The data in Table 4 indicate that approximately 4 (±2) mol%[2] olivine crystallized over a 48° interval (1248–1240°C). The curve in Fig. 5a shows that this was readily detected by the calorimeter. Electron microprobe analyses indicate that the composition of the olivine ranges between Fo_{96} and Fo_{94} (the high forsterite content is a consequence of running the experiments in air). The heat of fusion of Fo_{95} over the temperature range of 1248 to 1200°C can be calculated from the heats of fusion of pure forsterite (~142 kJ/mol at its melting point of 1901°C; Richet et al. 1993) and pure fayalite (89.3 kJ/mol at the metastable congruent melting point of 1217°C; Stebbins and Carmichael 1984). Extrapolation of these values to the temperature range of interest was accomplished using the heat capacity for crystalline forsterite and fayalite of Berman (1988) and the heat capacity for liquid Mg_2SiO_4 and liquid Fe_2SiO_4 calculated from the algorithm of Lange and Navrotsky (1992); these calculations led to a heat of fusion for Fo_{95} of ~74.6 kJ/mol between 1244 and 1200°C. Crystallization of ~4 (±2) mol% olivine over a 48°C interval, during cooling at 3°/min, corresponds to crystallization of ~1.3 mol% olivine in 5 min. Therefore, given the heat of fusion of Fo_{95} of ~74.6 kJ/mol, the results indicate that ~1.0 kJ per 5 min increment can be resolved. The uncertainty in this estimate caused by errors in the estimated modal abundance of olivine is approximately ±0.4 kJ.

We can test this estimate using the crystallization of leucite in the ugandite scans. During the 1°/min heating scan, ~16 mol% leucite and ~5 mol% clinopyroxene still remains in the sample by 1209°C. Additional quench experiments on the ugandite sample cooled at 1°/min show that <1% clinopyroxene and ~10 mol% leucite is present in the charge at 1220°C and that <4 mol% leucite is present in the charge at 1250°C. Therefore, between 1250 and 1220°C, approximately 6 mol% of leucite melted and was *not* detected in the calorimetric signal. We can estimate the heat of fusion for leucite using the value suggested by Ghiorso and Carmichael (1987) of −3.05 kJ/mol at room temperature (a correction of 10 kJ/mol from the value given by Kelley 1960). Extrapolation of this value up to 1250–1220°C was achieved using the heat capacity for crystalline leucite of Robie (1978) and Lange et al. (1986), and the heat capacity for liquid $KAlSi_2O_6$ using the algorithm of Lange and Navrotsky (1992); these calculations led to a heat of fusion for leucite of ~80.5 kJ/mol at 1235°C. Crystallization of ~6 (±2) mol% leucite over a 30°C interval, during a heating rate of 1°/min, corresponds to ~1.0 mol% leucite over a 5 min interval. Using the heat of fusion of ~80.5 kJ/mol for leucite indicates that the production of ~0.81 kJ per 5 min increment could *not* be resolved. Given the error in this estimate of approximately ±0.4 kJ, as well as the results presented above for olivine, the detection limit is probably not less than 0.6 kJ and not more than 1.2 kJ per 5 min increment. This range is within the detection limit estimated by Lange et al. (1991) of 1–1.2 kJ per 5 min interval, based on cooling scans (1°/min) of diopside liquid.

Conclusions

Continuous scanning experiments provide a "snapshot" picture of the instaneous release (or absorption) of enthalpy, and can thus be applied to studies of crystal-

[2] Uncertainites in modal abundance are small (±2 modal %) when only one mineral phase (not including spinel which is very bright in a back-scattered image) is present.

lization and melting as a function of cooling and heating rate. Kinetic information can only be obtained, however, when the detection limit of the calorimeter (between 0.6–1.2 kJ per 5 min increment) is taken into account. The important parameter is the release or absorption of heat *per unit time*, thus rapid scans tend to give sharper profiles relative to slow ones.

In contrast, step-scanning calorimetry can be readily applied to complex, multicomponent systems such as magmas to provide in-situ quantitative measurements of enthalpy across the liquidus-solidus interval. Such measurements provide detailed information on the distribution of latent heat during melting and crystallization that cannot be obtained by conventional drop calorimetry. These data are critical for models describing the thermal evolution of cooling magma bodies.

Acknowledgements This research was supported by the National Science Foundation (grant EAR-9104923). The electron microprobe facility at the University of Oregon was funded by grants from the National Science Foundation (EAR-9204446) and the W.M. Keck Foundation. The electron microprobe facility at the University of Michigan was funded by grant EAR-8212764 from the National Science Foundation.

References

Berman RG (1988) Internally consistent thermodynamic data for minerals in the system K_2O-Na_2O-CaO-MgO-FeO-Fe_2O_3-Al_2O_3-SiO_2-TiO_2-H_2O-CO_2. J Petrol 29:445–522

Brandeis G, Jaupart C, Allegre CJ (1984) Nucleation, crystal growth and the thermal regime of cooling magmas. J Geophys Res 89:10,161–10,177

Brown, FH (1971) Volcanic petrology of the Toro-Ankole region, western Uganda. PhD thesis, University of California, Berkeley

Carslaw HS, Jaeger JC (1959) Conduction of heat in solids, 2nd edn. Oxford University Press, Oxford

Cashman KV (1993) Relationship between plagioclase crystallization and cooling rate in basaltic melts. Contrib Mineral Petrol 113:126–142

Delaney PT (1988) Fortran 77 programs for conductive cooling of dikes with temperature-dependent thermal properties and heat of crystallization. Comp Geosci 14:181–212

DeYoreo JJ, Lux DR, Guidotti CV (1989) The role of crustal anatexis and magma migration in the thermal evolution of regions of thickened continental crust. In: Daly JS, Cliff RA, Yardley BWD (eds) Evolution of metamorphic belts. Geol Soc London Spec Publ 43:187–202

Ghiorso MS (1991) Temperatures in and around cooling magma bodies. In: Perchuk LL (ed) Progress in metamorphic and magmatic petrology. Cambridge University Press, Cambridge, pp 387–410

Ghiorso MS, Carmichael ISE (1987) Modeling magmatic systems: petrologic applications. In: Carmichael ISE, Eugster HP (eds) Thermodynamic modeling of geological materials (Reviews in Mineralogy, vol. 17). ch-pp 467–499

Ghiorso MS, Carmichael ISE, Rivers ML, Sack RO (1983) The Gibbs free energy of mixing of natural silicate liquids: an expanded regular solution approximation for the calculation of magmatic intensive variables. Contrib Mineral Petrol 84:107–145

Jaeger JC (1959) Temperatures outside a cooling intrusive sheet. Am J Sci 257:44–54

Jaeger JC (1961) The cooling of irregularly shaped igneous bodies. Am J Sci 259:721–734

Kelley KK (1960) Contributions to the data on theoretical metallurgy. XIII. High temperature heat content, heat capacity, and entropy data for the elements and inorganic compounds. US Bur Mines Bull 584

Kilinc A, Carmichael ISE, Rivers ML, Sack RO (1983) The ferric-ferrous ratio of natural silicate liquids equilibrated in air. Contrib Mineral Petrol 83:136–140

Lange RA, Navrotsky A (1992) Heat capacities of Fe_2O_3-bearing silicate liquids. Contrib Mineral Petrol 110:311–320

Lange RA, Carmichael ISE, Stebbins JF (1986) Phase transitions in leucite ($KAlSi_2O_6$), orthorhombic $KAlSiO_4$, and their iron analogues ($KFeSi_2O_6$, $KFeSiO_4$). Am Mineral 71:937–945

Lange RA, DeYoreo JJ, Navrotsky A (1991) Scanning calorimetric measurement of heat capacity during incongruent melting of diopside. Am Mineral 76:904–912

Larsen ES (1945) Time required for the crystallization of the great batholith of southern and lower California. Am J Sci 243A:399–416

Lovering TS (1936) Heat conduction in dissimilar rocks and the use of thermal models. Geol Soc Am Bull 47:87–100

Richet P, Bottinga Y (1984) Anorthite, andesine, wollastonite, diopside, cordierite and pyrope: thermodynamics of melting, glass transitions, and properties of the amorphous phases. Earth Planet Sci Lett 67:415–432

Richet P, Leclerc F, Benoist L (1993) Melting of forsterite and spinel, with implications for the glass transition of Mg_2SiO_4 liquid. Geophys Res Lett 20:1675–1678

Robie RA, Hemingway BS, Fisher JR (1978) Thermodynamic properties of minerals and related substances at 298.15 K and 1 bar (10^5 pascals) pressure and at high temperatures. US Geol Surv Bull 1452

Spohn T, Hort M, Fisher H (1988) Numerical simulation of the crystallization of multicomponent melts in thin dikes or sills 1. The liquidus phase. J Geophys Res 93:4880–4894

Stebbins JF, Carmichael ISE (1984) The heat of fusion of fayalite. Am Mineral 69:292–297

Stebbins JF, Carmichael ISE, Weill DE (1983) The high temperature liquid and glass heat contents and the heats of fusion of diopside, albite, sanidine and nepheline. Am Mineral 68:717–730

Wickham SM (1987) The segregation and emplacement of granitic magmas. J Geol Soc Lond 144:281–297

Wyllie PJ (1977) Crustal anatexis: an experimental review. Tectonophysics 43:41–71